


# Time-dependent broken-symmetry density functional theory simulation of the optical response of entangled paramagnetic defects: Color centers in lithium fluoride

Benjamin G. Janesko\*

Department of Chemistry &amp; Biochemistry, Texas Christian University, 2800 South University Drive, Fort Worth, Texas 76129, USA

 (Received 1 August 2017; revised manuscript received 2 December 2017; published 21 February 2018)

Parameter-free atomistic simulations of entangled solid-state paramagnetic defects may aid in the rational design of devices for quantum information science. This work applies time-dependent density functional theory (TDDFT) embedded-cluster simulations to a prototype entangled-defect system, namely two adjacent singlet-coupled  $F$  color centers in lithium fluoride. TDDFT calculations accurately reproduce the experimental visible absorption of both isolated and coupled  $F$  centers. The most accurate results are obtained by combining spin symmetry breaking to simulate strong correlation, a large fraction of exact (Hartree-Fock-like) exchange to minimize the defect electrons' self-interaction error, and a standard semilocal approximation for dynamical correlations between the defect electrons and the surrounding ionic lattice. These results motivate application of two-reference correlated *ab initio* approximations to the M-center, and application of TDDFT in parameter-free simulations of more complex entangled paramagnetic defect architectures.

DOI: [10.1103/PhysRevB.97.085138](https://doi.org/10.1103/PhysRevB.97.085138)

## I. INTRODUCTION

Optically addressable paramagnetic defects in wide-band-gap semiconductors and insulators show enormous promise for quantum information science [1]. Such defects have been used as qubits for quantum computing [2–4], fluorescent probes [5] and sensors [6], narrowband single-photon emitters [7], and nanoscale magnetometers [8,9]. Atomistic *ab initio* simulations of such defects' structure [10], optical response [11,12], and quantum-mechanical entanglement are critical for interpreting experiments. Such simulations could ultimately aid rational design of practical devices [13,14]. This fact motivates the development and testing of accurate, minimally empirical, and computationally efficient approaches for atomistic simulation of such defects.

A simple model system of optically addressable paramagnetic defects is alkali halide F-centers (color centers), in which a single electron is trapped at an anion vacancy [15–17]. The trapped electron forms a “quasiatom” analogous to a hydrogen atom [18]. Atomistic simulations have confirmed the anion-vacancy model of the F-center [16], characterized the detailed structure of its electron density [19], and provided accurate treatments of its geometry [20] and optical spectra [21,22]. An important recent study demonstrated that both embedded-cluster *ab initio* quantum chemistry and periodic supercell many-body perturbation theory ( $GW+BSE$ ) [22] provide quantitative agreement with the experimental absorption spectra of isolated F-centers [23]. Follow-up studies give insight into the Mollwo-Ivey relation between lattice parameter and absorption energy [24].

I recently showed [25] that the lithium fluoride M-center defect, a “quasi- $H_2$  molecule” with two singlet-coupled electrons trapped at adjacent anion vacancies [26,27], provides a

simple and experimentally realized model system for entanglement among optically addressable paramagnetic defects. The M-center is analogous to the singlet ground state of  $H_2$  with a stretched H-H bond, a “textbook” system for strong correlation and entanglement [28–35]. This system's singlet ground state at the limit of a long bond length is the maximally entangled two-qubit state  $|\Psi^+\rangle = \frac{1}{\sqrt{2}}(|\uparrow\downarrow\rangle + |\downarrow\uparrow\rangle)$  invoked in quantum information science [36]. Simple molecular-orbital/band-structure pictures (single-reference symmetry-restricted Hartree-Fock calculations) qualitatively fail to reproduce the M-center's experimental ground-state magnetization and absorbance spectrum [37,38], just as they qualitatively fail to reproduce the excitation energies of stretched  $H_2$  [39]. However, Ref. [25] showed that a broken-spin-symmetry time-dependent Hartree-Fock treatment of the first singlet excitation energy, “dressed” with approximate corrections for electron correlation [23], predicted an M-center absorbance peak within  $\sim 0.3$  eV of experiment [25]. Improved *ab initio* results would in principle require correlated multireference calculations, whose computational expense makes them impractical for large-scale simulations of realistic device architectures.

Kohn-Sham density functional theory (DFT) has been widely applied as a solution to such difficulties. DFT simulations, using relatively simple density functional approximations (DFAs) for the exact exchange-correlation functional, combine mean-field cost with useful accuracy for many systems [40–42]. Hybrid DFAs incorporating a fraction of exactly computed (Hartree-Fock-like, HF) exchange are particularly popular, as they tune the “zero-sum” tradeoff between electron self-interaction and simulation of electron correlation in covalent bonds [31]. Broken-spin-symmetry Kohn-Sham calculations using wave functions that are not eigenfunctions of  $\hat{S}^2$  (i.e., that are not pure singlet, doublet, triplet, etc. states) can sometimes treat properties that would otherwise require multireference *ab initio* theory [43]. Reference [25] reviews the classic example of the singlet ground-state energy of stretched

\*b.janesko@tcu.edu

$H_2$ . This is above the triplet energy in symmetry-restricted calculations with standard DFAs and Hartree-Fock theory, but qualitatively correct in broken-symmetry calculations placing spin-up and spin-down electrons on different atoms. An enormous range of spin-projection and effectively multireference methods have been proposed to connect broken-symmetry DFT calculations back to states of the desired symmetry [44–49]. (Specialists may note the argument that the exact ground-state wave function of the noninteracting Kohn-Sham reference system need not be an eigenfunction of  $\hat{S}^2$ , or of any other two-electron operator [50].) Practical applications of broken-symmetry DFT are exemplified in recent treatments of magnetic couplings [51].

DFT is also applied beyond the ground state [52]. Adiabatic linear-response time-dependent density functional theory (TDDFT) calculations, performed using standard ground-state DFAs, can accurately simulate the character and vertical excitation energy of many singly excited states [53–56]. References [57,58] review connections between TDDFT and the many-body Green’s function approaches applied in Ref. [23]. The combination of TDDFT and spin symmetry breaking is particularly powerful for multireference systems. TDDFT excitations computed from broken-symmetry singlet ground states have been recently applied to long-range charge-transfer excitations [59] and electronic spectra of open-shell singlet diradical nickel complexes [60]. CI-singles (Tamm-Dancoff) Hartree-Fock calculations from broken-symmetry ground states provide qualitatively reasonable singlet excitation energies for dissociating  $H_2$ , though they can be problematic for triplet states [61]. TDDFT from symmetry-unrestricted paramagnetic states has also been applied to optical absorption spectra of oxo and peroxo dicopper(II) complexes [62], dynamic polarizability of open-shell molecular systems [63], and electronic circular dichroism spectra of open-shell Cr(III) compounds [64]. Other relevant work includes spin-flip TDDFT treatments of ground states [65,66], the linear response of projected Hartree-Fock theory [49,67] and noncollinear spin density functional theory [68], and the use of broken-symmetry wave functions as reference in semiempirical CI singles [69].

This work reports the performance of broken-symmetry embedded-cluster TDDFT calculations, using various approximate DFAs, in simulating the electronic structure and absorption spectra of isolated paramagnetic F-centers and strongly correlated adjacent singlet-coupled F-centers. While Hartree-Fock theory itself tends to overestimate the excitation energies, DFAs incorporating large fractions of HF exchange provide balanced treatments of both F- and M-centers. The minimally empirical long-range-corrected DFA LC- $\omega$ PBE, and a screened hybrid DFA combining 100% screened HF exchange with long-range PBE exchange, provide balanced performance for both systems. This motivates applying broken-symmetry TDDFT to simulate more complicated coupled-defect architectures relevant to quantum information science.

## II. COMPUTATIONAL METHODS

This work uses the development version of the GAUSSIAN suite of programs [70] to perform generalized Kohn-Sham calculations with nonlocal, nonmultiplicative exchange-correlation potentials for DFAs incorporating HF exchange

[71,72]. Computational details closely follow the embedded-cluster calculations of Ref. [25], with a more sophisticated extrapolation to the basis set and cluster embedding limits. Atomic positions are taken from defect-free lattices at the experimental LiF lattice constants 2.02 Å [73]. The single F-center is treated as a  $Li_{14}F_{12}^+$  cluster treated completely quantum mechanically (QM) [37]. This cluster is surrounded by a  $Li_{150}F_{128}$  cluster of embedding potentials, then by a  $Li_{2026}F_{2048}$  cluster of isolated point charges  $\pm 1$  (cluster “F1”). The M-center lying along the  $\langle 110 \rangle$  direction is treated as a  $Li_{10}F_{18}^{-10}$  QM cluster, embedded in a surrounding  $Li_{136}F_{150}$  cluster of embedding potentials, surrounded by a  $Li_{3730}F_{3704}$  cluster of isolated point charges (cluster “M1”). As in Ref. [25], calculations treat the  $Li^+$  embedding potential as a point charge +1 surrounded by the SBKJC effective core potential (ECP) [74], and they treat the  $F^-$  embedding potential as a point charge  $-1$  surrounded by the SBKJC ECP of  $Na^+$ . While the assumption that 10-electron ions  $F^-$  and  $Na^+$  have identical cores is clearly imperfect, Ref. [25] showed that calculations with this assumption largely reproduce previous work, suggesting that the detailed form of the embedding potential is not critical for the effects of interest here. Unless noted otherwise, calculations use the cc-pVDZ basis set on the QM region, and include “dummy” hydrogen atom basis sets at the defect centers.

The embedded-cluster calculations F1 are extrapolated as follows. The time-dependent unrestricted Hartree-Fock/cc-pVDZ first excitation energy of cluster F1 is 6.2255 eV, versus 6.1672 eV for much larger embeddings up to  $Li_{1672}F_{1732}$  embedding potentials and  $Li_{504}F_{444}$  point charges, giving a 0.06 eV redshift for the embedding potential. Calculations with larger QM regions give first excitation energies 6.1672 eV  $Li_{14}F_{12}$ , 6.1043 eV  $Li_{14}F_{18}$ , 6.0680 eV  $Li_{38}F_{18}$ , and 6.0489 eV  $Li_{38}F_{54}$ . Extrapolation as  $N^{-1}$ , where  $N$  is the number of atoms in the QM region, suggests a QM-cluster limit excitation energy 6.02 eV and a 0.15 eV redshift to extrapolate the QM region. Calculations on the F1 cluster give excitation energies 6.0738 eV in the cc-pVTZ basis set and 6.0488 eV in the cc-pVQZ basis set. Extrapolation as  $Z^{-3}$ , where  $Z$  is the basis-set cardinality, suggests a basis-set limit value 6.03 eV and a 0.13 eV redshift for basis-set corrections to the F1/cc-pVDZ results. Combined, these suggest a  $0.06 + 0.15 + 0.13 = 0.34$  eV total redshift to F1/cc-pVDZ results to reach the basis-set and cluster-size limit. This shift is smaller than the  $(5.99-5.50) = 0.45$  eV redshift between  $Li_{14}F_{12}$ /cc-pVDZ and  $Li_{62}F_{62}$  complete basis-set CASPT2(ROHF) results reported in Ref. [23], consistent with the larger basis-set demands of the latter’s correlated *ab initio* calculations. Additional redshifts of 0.21 eV for ground- and excited-state geometry relaxation and 0.09 eV for electron-phonon coupling are taken from Ref. [23].

The embedded-cluster calculations M1 are extrapolated as follows. The broken-symmetry time-dependent unrestricted Hartree-Fock/cc-pVDZ first excitation energy of cluster M1 is 4.1835 eV, versus 4.1834 eV for much larger embeddings up to  $Li_{136}F_{150}$  embedding potentials and  $Li_{6934}F_{6908}$  point charges, giving negligible redshifts for embedding potential. Calculations with larger QM regions give first excitation energies 4.1835 eV  $Li_{10}F_{18}$ , 4.1478 eV  $Li_{22}F_{18}$ , and 4.1285 eV  $Li_{22}F_{26}$ . Extrapolation as  $N^{-1}$  suggests a QM-cluster limit excitation energy 4.05 eV and a 0.13 eV redshift to extrapolate the QM region. Broken-symmetry TDUHF calculations on

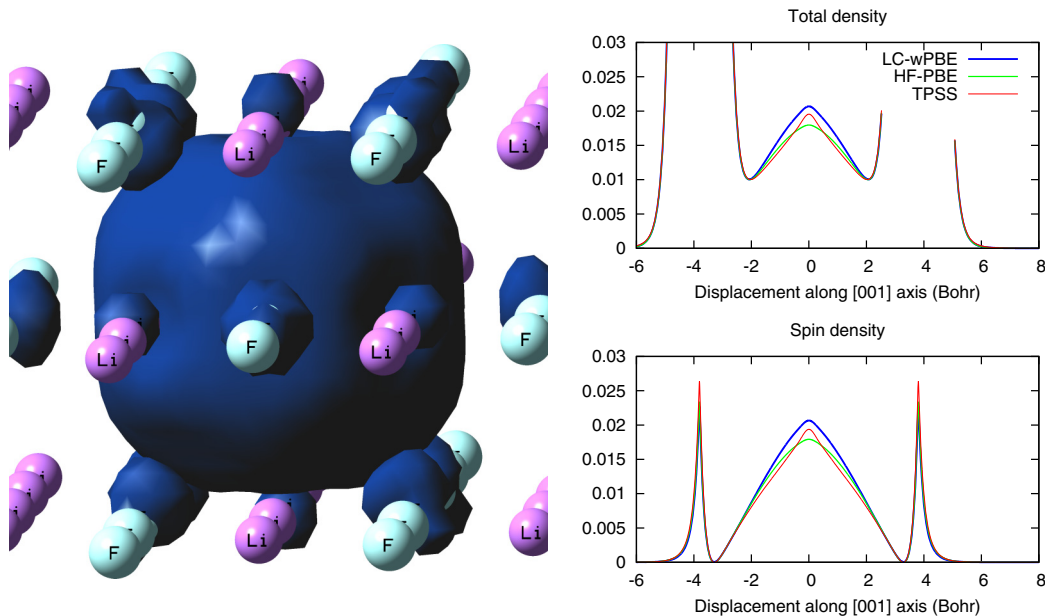


FIG. 1. Structure and spin density of an isolated F-center defect. Left: three-dimensional structure and LC- $\omega$ PBE spin density, isosurface  $0.0004 \text{ bohr}^{-3}$ . Right: defect total and spin densities along along the [100] axis, evaluated for representative DFAs.

the M1 cluster give excitation energies 4.1459 eV in the cc-pVTZ basis and 4.1273 eV in the cc-pVQZ basis, such that extrapolation as  $Z^{-3}$  gives a basis-set limit 4.12 eV and a 0.06 eV redshift for basis-set corrections to M1/cc-pVDZ results. These basis-set effects for the M-center  $^1\Sigma_g^+ \rightarrow ^1\Sigma_u^+$  excitation are smaller than the basis-set effects on the F-center  $1s \rightarrow 2p$  excitation, as expected. Combined, these suggest an  $0.13 + 0.06 = 0.18$  eV total redshift to M1/cc-pVDZ results to reach the basis-set and cluster-size limit. Additional redshifts of 0.21 eV for ground- and excited-state geometry relaxation and 0.09 eV for electron-phonon coupling are assumed to be identical to those of the F-center.

A major part of this work involves comparing the performance of different DFAs. Calculations compare a broad range of “standard” DFAs implemented in the GAUSSIAN package [70]. The simplest tested approximations are the local spin-density approximation (LSDA) [75] and the  $X\alpha$  method combining rescaled LSDA exchange and no correlation functional [76]. Tested generalized gradient approximations (GGAs) include the nonempirical Perdew-Burke-Ernzerhof (PBE) and Perdew-Wang PW91 GGAs [77,78] and the empirical B97-1 [79], B97-2 [80], B97-D [81], HCTH93 [82], HCTH147 [83], and HCTH407 [84] GGAs. (While empirical dispersion corrections as in B97-D are not expected to significantly affect the present results, their importance in other areas [85] motivates inclusion here.) Tested meta-GGAs include the nonempirical Tao-Perdew-Staroverov-Scuseria (TPSS) [86] and empirical M06-L [87]. Tested global hybrids including a constant fraction of HF exchange include the arguably nonempirical [88] PBE0 (25% HF exchange) [89,90] and the empirical O3LYP (11.6%) [91], B3LYP (20%) [78,92–95], BHHLYP (50%) [78,92,93], and M06-HF (100%) [96] global hybrids. Calculations also test the combination of 100% HF exchange with the LDA or PBE correlation functional, denoted “HFLDA” or “HFPBE,” and the APFD combination of 41.1%

B3PW91 and 58.9% PBE0 plus dispersion corrections [97]. Tested range-separated hybrids include the HSE06 [98,99] and HISS [100] screened hybrids incorporating no long-range HF exchange, as well as a “HSE100” combining 100% short-range HF exchange with no long-range HF exchange. Tested long-range-corrected hybrids, whose inclusion of additional long-range HF exchange is known to improve many excited states [101], include LC- $\omega$ PBE [102],  $\omega$ B97X-D [103], and CAM-B3LYP [104].

Other computational details are as follows. TDDFT calculations are performed with versus without the Tamm-Dancoff approximation. Calculations on the M-center are performed from both symmetric and broken-spin-symmetry singlet states. The broken-spin absorption is assumed to correspond to the first excited state with a non-negligible computed transition dipole moment. All corrections are assumed to be transferable between the tested DFT methods, and between TD, TDA, and band-structure calculations. All excitations are confirmed to be dipole-allowed states with significant nonzero predicted transition dipole moments. Atom-averaged quantities are obtained using Mulliken population analysis.

### III. RESULTS

#### A. Isolated paramagnetic defect

Figure 1 presents a single F-center’s three-dimensional fine structure and ground-state spin density, as well as total and spin densities inside the defect computed with representative DFAs. The unpaired electron density is localized inside the defect, yielding a non-nuclear attractor [19] in the total density.

Table I includes additional detail on different DFAs’ predictions for the F-center defect electronic structure. The table includes the total electron density at the non-nuclear attractor  $\rho_{\text{NNA}}$ , and the total Mulliken charge and spin density  $\text{Li}_Q$  and  $\text{Li}_M$  of the lithium atoms adjacent to the defect. DFAs that

TABLE I. Excitation energies (eV) of a single isolated F-center, predicted using a variety of density functional approximations. Results are shown for time-dependent density functional theory (TDDFT), the Tamm-Dancoff approximation (TDA), and band energies (“Band”). Isolated hydrogen atom  $1s \rightarrow 2p$  TD excitation energy “H atom,” total density at the non-nuclear attractor  $\rho_{\text{NNA}}$  (a.u.), and atom-averaged partial charge  $\text{Li}_Q$  and spin  $\text{Li}_M$  for the Li atoms closest to the defect are included. DFAs are sorted from smallest to largest predicted TDDFT excitation energy.

Method	TDDFT	TDA	Band	H atom	$\rho_{\text{NNA}}$	$\text{Li}_Q$	$\text{Li}_M$
Experiment	5.08						
LDA	4.24	4.3	3.85	9.87	1.57	0.558	0.160
BLYP	4.33	4.38	4.14	10.18	1.809	0.625	0.123
B97D	4.35	4.43	4.19	10.53	1.462	0.69	0.109
HFS	4.39	4.45	4.02	9.71	1.626	0.536	0.154
PW91	4.44	4.49	4.17	10.34	1.641	0.63	0.13
PBE	4.46	4.51	4.17	10.24	2.069	0.632	0.13
HCTH407	4.58	4.67	4.28	10.46	2.069	0.665	0.143
B3LYP	4.62	4.67	5.69	10.4	1.829	0.661	0.118
X3LYP	4.63	4.68	5.8	10.42	1.828	0.657	0.118
B972	4.67	4.72	5.75	10.64	1.614	0.715	0.112
O3LYP	4.68	4.73	5.23	10.46	1.718	0.689	0.121
HSE	4.76	4.81	5.3	10.5	1.655	0.679	0.118
APFD	4.77	4.78	5.97	10.49	1.677	0.685	0.12
CAMB3LYP	4.79	4.84	8.39	10.4	1.818	0.639	0.122
PBE0	4.79	4.84	6.11	10.51	1.663	0.683	0.12
B971	4.8	4.86	5.74	10.56	1.993	0.68	0.129
TPSS	4.85	4.92	4.78	10.48	1.955	0.68	0.114
$\omega$ B97XD	4.93	5.02	9.53	10.39	1.944	0.69	0.135
BHHLYP	4.95	5	8.02	10.71	1.883	0.714	0.104
HISS	4.98	5.03	5.82	10.74	1.72	0.677	0.109
LC- $\omega$ PBE	5.06	5.12	10.86	10.53	2.069	0.636	0.119
HFTSS	5.35	5.43	11.8	11.18	1.6	0.827	0.089
HSE100	5.38	5.43	8.91	11.31	1.823	0.831	0.086
HFLDA	5.4	5.45	12.23	11.45	2.017	0.843	0.081
HFPBE	5.43	5.49	12.05	11.32	1.797	0.829	0.089
HF	5.53	5.59	12.45	11.24	2.069	0.828	0.071

localize the trapped electron inside the defect tend to give  $\text{Li}_Q$  approaching +1, and  $\text{Li}_M$  approaching 0.

Table I also presents the predicted symmetry-unrestricted TD and TDA first excitation energies of a single F-center. Band-structure excitation energies (highest occupied molecular orbital–lowest unoccupied molecular orbital gaps) and TD first excitation energies of an isolated H atom are reported for comparison. Figure 2 summarizes the errors relative to experiment. Results are sorted from lowest to highest F-center TD excitation energy. These spin-unrestricted doublet calculations have little spin contamination, with ground and excited state  $\langle \hat{S}^2 \rangle$  between 0.750 and 0.754. All of the tested DFAs predict that the F-center excitation is a ( $1s \rightarrow 2p$ )-like excitation of the trapped electron “quasiatom.”

The trends for single trapped electrons in Table I and Fig. 2 are consistent with the previous literature on time-dependent DFT. The best agreement with experiment comes from DFAs that combine a semilocal correlation functional with a large fraction of HF exchange, particularly the long-range-corrected LC- $\omega$ PBE. TD and TDA results are nearly identical, consistent with previous studies of the Tamm-Dancoff approximation [105]. Band energies do not reproduce the experimental ab-

sorption energy, consistent with their lack of particle-hole interactions [23,106]. Similar results are found for the M-center (not shown).

The trends among different DFAs are also broadly consistent with the literature. Time-dependent Hartree-Fock calculations (entry “HF”) give an absorption energy  $\sim 0.5$  eV above experiment. This is consistent with the important role of dynamical correlation seen in Refs. [20,23]. (The TDHF F-center calculations in Ref. [25], unlike the present calculations, included an approximate correction for dynamical correlation extrapolated from the *ab initio* calculations in Ref. [23].) Adding semilocal correlation corrections to Hartree-Fock theory (entries “HFLDA” and “HFPBE”) modestly improves the predicted F-center excitation energies. In contrast to these full-range HF results, DFAs that do not include any HF exchange underestimate the excitation energy. This is consistent with these DFAs’ known self-interaction error [107] and their resulting tendency to underestimate valence and Rydberg excitations [56]. However, it is important to note that long-range HF exchange is not required to accurately predict the F-center excitation energy. This conclusion is particularly encouraging for periodic supercell simulations of paramagnetic defects, as long-range HF exchange can be computationally expensive in such simulations [108]. The “middle-range” HISS hybrid gives an excitation energy close to LC- $\omega$ PBE. The HSE100 hybrid of 100% screened HF exchange approaches HFPBE (100% full-range HF exchange). This is again consistent with the literature on range separation in DFAs, particularly Ref. [109]. That reference demonstrated that many properties of interest, particularly in condensed phases, depend on the “middle-range exchange” between electrons separated by  $\sim 1$ – $2$  bohr (or equivalently one to two chemical bond lengths). For many properties, including low-lying Rydberg state excitations, polarizabilities of  $\text{H}_2$  chains, and Raman activities, screened hybrid DFAs incorporating no asymptotic long-range HF exchange can provide performance comparable to long-range-corrected hybrids incorporating 100% asymptotic long-range HF exchange. (However, truly “long-range” properties such as long-range between-molecule charge transfer do still require long-range HF exchange [110].)

Reference [25] illustrated the utility of comparing the F-center “quasiatom” to the hydrogen atom itself. Accordingly, Table I also reports the first bright state excitation predicted for the H atom. Trends in the different DFAs’ predictions for the F-center excitation energy generally mirror trends for the hydrogen atom. This is consistent with the “quasiatom” model of the F-center as a single electron confined by the surrounding ionic lattice [18].

Additional insight comes from the trends in electron density in Table I. DFAs that localize the trapped electron inside the vacancy, and give  $\text{Li}_Q$  near 1 and  $\text{Li}_M$  near 0, also tend to give relatively large excitation energies, as expected from their enhanced localization. In contrast, the computed total density at the NNA proves to have a weaker correlation with the predicted excitation energies.

## B. Adjacent singlet-coupled defects

Figure 3 presents two singlet-coupled F centers’ three-dimensional structure and ground-state spin density, evaluated

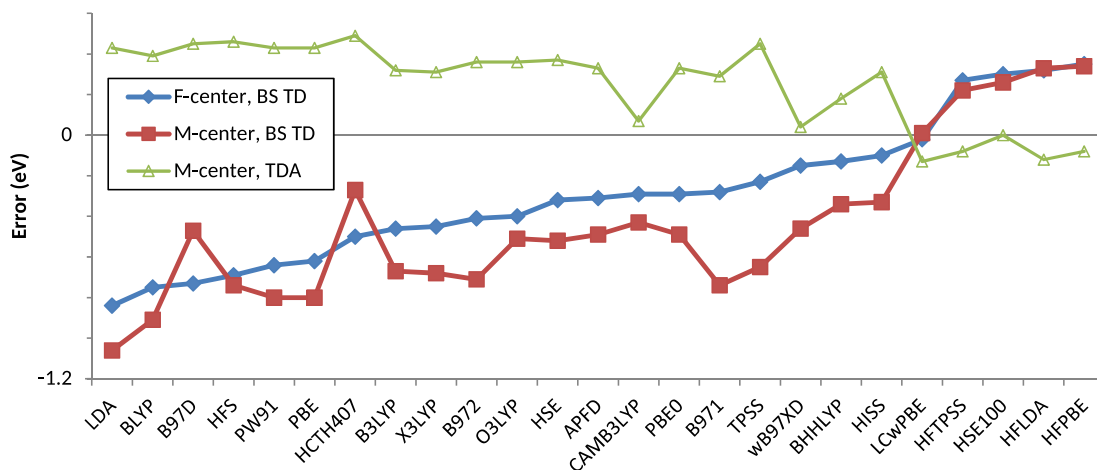


FIG. 2. Signed error (theory-experiment, eV) in the excitation energies of F- and M-centers predicted by time-dependent DFT using various DFAs. Results are shown for broken-symmetry TD calculations on an isolated F-center, and broken-symmetry TD and symmetry-restricted TDA calculations on an M-center.

with broken-symmetry DFT. The effect of symmetry breaking is clear: one defect site contains mostly  $\alpha$ -spin electrons, the other contains mostly  $\beta$ -spin electrons. Table II presents the computed Mulliken charge and spin density  $Li_Q$  and  $Li_M$  of the four Li atoms closest to the left F-center. The variations among different DFAs are somewhat larger than for the isolated F-center (Table I). Increasing the fraction of HF exchange increases the spin polarization, increasing both the charge and spin on the atoms.

Table III presents the predicted symmetry-restricted and broken-symmetry TD and TDA first excitation energies of the two adjacent singlet-coupled defects in the M-center. Figure 2 summarizes the signed errors in F-center TD, M-center symmetry-restricted TDA, and M-center spin-broken-

symmetry (BS) TD approximations. In symmetry-restricted calculations, all tested DFAs give singlet  $\rightarrow$  triplet excitations with negative excitation energies, consistent with previous evidence that the M-center has a singlet-triplet instability comparable to  $H_2$  stretched beyond the Coulson-Fischer point [25,37].

The symmetry-restricted TD and TDA excitation energies depend only modestly on the choice of DFA. DFAs with large fractions of HF exchange tend to predict TD and TDA excitation energies below those of DFAs without HF exchange. This trend is consistent with the results seen in Table III for stretched  $H_2$ . The TDA first singlet excitation energies are higher and somewhat more accurate than TD. The rather good performance of symmetry-restricted TDA for the

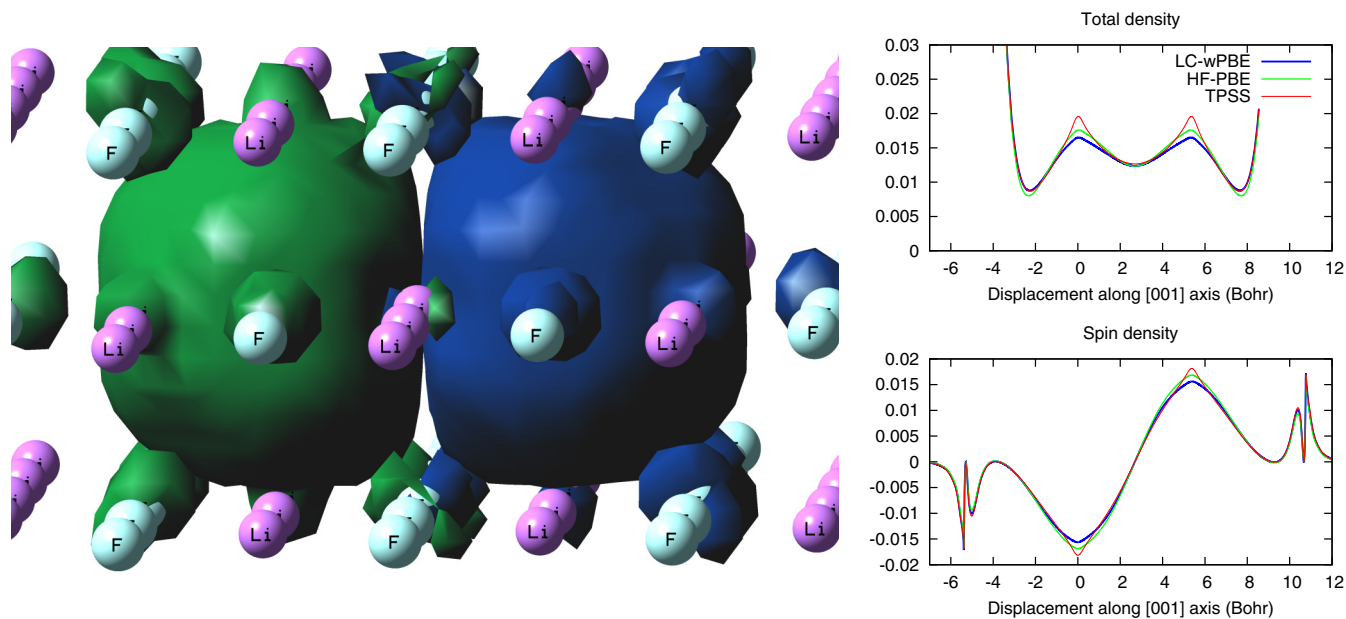


FIG. 3. Structure and spin density of two coupled F-center defects. Left: three-dimensional structure and LC- $\omega$ PBE spin density, isosurface 0.0004 bohr<sup>-3</sup>. Blue and green denote different spin polarizations. Right: defect total and spin densities along along the [110] axis, evaluated for representative DFAs.

TABLE II. Atom-averaged partial charge  $Li_Q$  and spin  $Li_M$  for the Li atoms closest to the left defect, in two adjacent singlet-coupled F-center defects. DFAs are sorted from smallest to largest predicted  $Li_Q$ .

Method	$Li_Q$	$Li_M$
HFS	-0.096	0.250
LDA	-0.065	0.199
BLYP	0.011	0.189
PW91	0.024	0.204
PBE	0.026	0.205
LC- $\omega$ PBE	0.072	0.212
CAMB3LYP	0.073	0.210
TPSS	0.078	0.194
X3LYP	0.087	0.199
B3LYP	0.090	0.199
B97D	0.103	0.178
SLC-PBE	0.107	0.211
B971	0.112	0.184
HSE	0.114	0.204
HCTH407	0.115	0.231
$\omega$ B97XD	0.117	0.209
APFD	0.124	0.207
HISS	0.126	0.200
PBE0	0.126	0.206
O3LYP	0.147	0.208
B972	0.151	0.173
BHHLYP	0.188	0.195
MN15L	0.225	0.157
HF	0.368	0.172
HFTPSS	0.372	0.188
HSE100	0.374	0.186
HFPBE	0.376	0.190
HFLDA	0.395	0.179

M-center excited state is comparable to that seen previously for symmetry-restricted CI-single calculations on  $H_2$  [61]. Overall, symmetry-restricted TDA excitations, computed using DFAs combining semilocal correlation with large fractions of HF exchange, tend to be rather accurate for the M-center.

In contrast to the case of unstable symmetry-restricted reference wave functions, the stable broken-symmetry excitation energies depend rather strongly on the choice of DFA. As for the F-center, TD and TDA results obtained with a given DFA are nearly identical [105]. Trends in different DFAs mirror those seen for the isolated F-center, as well as for isolated H atom and broken-symmetry  $H_2$ . In all of these cases, DFAs without HF exchange underestimate the excitation energy, while those with 100% HF exchange overestimate it.

Dynamical correlation proves to have a particularly large effect in broken-symmetry simulations of the M-center. Broken-symmetry TDHF strongly overestimates the M-center excitation energy, while the HFLDA, HFPBE, and HFTPSS combinations of HF exchange with a DFA for dynamical correlation are significantly more accurate. (The TDHF M-center calculations in Ref. [25], unlike the present calculations, included an approximate correction for dynamical correlation taken from Ref. [23].) This appears to result from an improved treatment of the trapped electrons' interactions with the defect

TABLE III. Excitation energies (eV) of a single M-center, predicted with a variety of density functionals and symmetry-restricted and broken-symmetry TD and TDA calculations. TD results for  $H_2$ , with bond length 2.85 Å equal to the M-center's defect-defect separation, are included for comparison.

Method	Symmetric			Symmetry-broken		
	TD	TDA	$H_2$	TD	TDA	$H_2$
Experiment	2.79					
LDA	1.84	3.25	3.48	1.76	2.25	4.03
BLYP	1.91	3.21	3.42	1.91	2.09	4.64
B97D	1.96	3.26	3.44	2.35	2.64	8.05
X $\alpha$	1.83	3.28	3.48	2.09	2.19	6.27
PW91	1.90	3.24	3.45	2.02	2.16	6.41
PBE	1.89	3.25	3.46	2.02	2.16	6.27
HCTH147	1.95	3.28	3.43	2.34	2.62	7.11
HCTH93	1.95	3.24	3.42	2.33	2.52	6.88
HCTH407	1.94	3.33	3.42	2.57	2.70	7.51
B3LYP	1.93	3.13	3.40	2.14	2.26	5.46
X3LYP	1.93	3.13	3.39	2.14	2.26	5.57
B972	1.95	3.18	3.41	2.10	2.41	8.63
O3LYP	1.94	3.18	3.39	2.29	2.37	4.90
HSE	1.93	3.19	3.41	2.31	2.41	7.16
APFD	1.93	3.15	3.42	2.32	2.42	6.87
CAM-B3LYP	1.87	2.89	3.37	2.38	2.47	5.96
PBE0	1.93	3.15	3.41	2.33	2.43	7.13
B971	1.94	3.09	3.41	2.06	2.41	8.22
TPSS	1.94	3.26	3.53	2.15	2.24	3.20
$\omega$ B97X-D	1.88	2.84	3.40	2.33	4.70	7.63
BHHLYP	1.95	3.00	3.32	2.47	2.55	6.57
HISS	1.94	3.12	3.35	2.49	2.88	7.94
LC- $\omega$ PBE	1.80	2.69	3.36	2.82	2.88	7.77
HFTPSS	1.88	2.74	2.96	3.02	3.09	8.67
HSE100	1.95	2.81	3.19	3.05	3.12	9.40
HFLDA	1.94	2.68	3.14	3.11	3.18	7.60
HFPBE	1.92	2.74	3.18	3.13	3.19	9.29
HF	1.95	2.75	3.17	3.69	3.77	9.38

walls. Broken-symmetry TD calculations on an isolated  $H_2$  molecule show a much smaller effect of the dynamical correlation functional: HF and HFPBE excitation energies differ by <0.1 eV for  $H_2$ , >0.5 eV for the M-center.

#### IV. DISCUSSION

The results presented here show that time-dependent DFT can provide accurate treatments of the optical response of both isolated and coupled paramagnetic defects in lithium fluoride. Density functional approximations that combine a large fraction of HF exchange with a standard semilocal approximation for dynamical correlation prove to give a balanced treatment of both the defect electron and its coupling with the surrounding ionic lattice. Careful extrapolation to the basis-set and cluster-size limits gives confidence in these embedded-cluster results.

Overall, the LC- $\omega$ PBE long-range-corrected DFA gives the best agreement with experiment, giving F-center, symmetry-restricted TDA M-center, and broken-symmetry TD M-center excitations all within 0.03 eV of the experimental values. This is consistent with the LC- $\omega$ PBE known accuracy for

valence, Rydberg, and charge-transfer excited states [102]. The “HSE100” combination of 100% screened HF exchange and semilocal correlation gives results nearly comparable to the full-range HF exchange HFPBE. This shows that long-range HF exchange is not necessary for simulating these localized trapped-electron defects, consistent with previous comparisons of screened versus long-range-corrected DFAs for some other properties improved by long-range correction [109].

The success of broken-symmetry DFT is consistent with the physical picture of the M-center defect as two strongly correlated trapped electrons, weakly correlated with the surrounding lattice. Broken-symmetry HF-PBE is from this perspective a broken-symmetry approximation to a two-component open-shell reference, combined with a simple DFT treatment of the

trapped electrons’ correlations with the surrounding crystal lattice. This further suggests that a relatively simple two-configuration wave function, combined with second-order many-body corrections, could provide accurate *ab initio* predictions for M-center excitations.

Overall, these results provide a framework for future atomistic simulations of coupled, optically addressable paramagnetic defects in quantum information science.

## ACKNOWLEDGMENT

This work was supported by US National Science Foundation DMR Grant No. 1505343.

- 
- [1] P. Neumann, N. Mizuochi, F. Rempp, P. Hemmer, H. Watanabe, S. Yamasaki, V. Jacques, T. Gaebel, F. Jelezko, and J. Wrachtrup, *Science* **320**, 1326 (2008).
- [2] M. V. Gurudev Dutt, L. Childress, L. Jiang, E. Togan, J. Maze, F. Jelezko, A. S. Zibrov, P. R. Hemmer, and M. D. Lukin, *Science* **316**, 1312 (2007).
- [3] W. F. Koehl, B. B. Buckley, F. J. Heremans, G. Causlone, and D. D. Awschalom, *Nature (London)* **479**, 84 (2011).
- [4] L. C. Bassett, F. J. Heremans, D. J. Christle, C. G. Yale, G. Burkard, B. B. Buckley, and D. D. Awschalom, *Science* **345**, 1333 (2014).
- [5] S.-J. Yu, M.-W. Kang, H.-C. Chang, K.-M. Chen, and Y.-C. Yu, *J. Am. Chem. Soc.* **127**, 17604 (2005).
- [6] A. L. Falk, P. V. Klimov, B. B. Buckley, V. Ivády, I. A. Abrikosov, G. Calusine, W. F. Koehl, A. Gali, and D. D. Awschalom, *Phys. Rev. Lett.* **112**, 187601 (2014).
- [7] V. Jacques, E. Wu, F. Grosshans, F. Treussart, P. Grangier, A. Aspect, and J.-F. Roch, *Science* **315**, 966 (2007).
- [8] J. R. Maze, P. L. Stanwix, J. S. Hodges, S. Hong, J. M. Taylor, P. Cappellaro, L. Jiang, M. V. G. Dutt, E. Togan, A. S. Zibrov, *et al.*, *Nature (London)* **455**, 644 (2008).
- [9] G. Balasubramanian, I. Y. Chan, R. Kolesov, M. Al-Hmoud, J. Tisler, C. Shin, C. Kim, A. Wojcik, P. R. Hemmer, A. Krueger, *et al.*, *Nature (London)* **455**, 648 (2008).
- [10] F. M. Hossain, M. W. Doherty, H. F. Wilson, and L. C. L. Hollenberg, *Phys. Rev. Lett.* **101**, 226403 (2008).
- [11] M. Bockstedte, A. Marini, O. Pankratov, and A. Rubio, *Phys. Rev. Lett.* **105**, 026401 (2010).
- [12] P. Delaney, J. C. Greer, and J. A. Larsson, *Nano Lett.* **10**, 610 (2010).
- [13] J. R. Weber, W. F. Koehl, J. B. Varley, A. Janotti, B. B. Buckley, C. G. Van de Walle, and D. D. Awschalom, *Proc. Natl. Acad. Sci. (USA)* **107**, 8513 (2010).
- [14] Y. Tu, Z. Tang, X. G. Zhao, Y. Chen, Z. Q. Zhu, J. H. Chu, and J. C. Fang, *Appl. Phys. Lett.* **103**, 072103 (2013).
- [15] F. Seitz, *Rev. Mod. Phys.* **18**, 384 (1946).
- [16] J. H. Schulman and W. D. Compton, *Color Centers in Solids* (Macmillan, New York, 1962).
- [17] J. Lambe and W. D. Compton, *Phys. Rev.* **106**, 684 (1957).
- [18] M.-S. Miao and R. Hoffmann, *J. Am. Chem. Soc.* **137**, 3631 (2015).
- [19] R. F. W. Bader and J. A. Platts, *J. Chem. Phys.* **107**, 8545 (1997).
- [20] V. V. Rybkin and J. Van de Vondelle, *J. Chem. Theor. Computat.* **12**, 2214 (2016).
- [21] F. Illas and G. Pacchioni, *J. Chem. Phys.* **108**, 7835 (1998).
- [22] P. Rinke, A. Schleife, E. Kioupakis, A. Janotti, C. Rodl, F. Bechstedt, M. Scheffler, and C. G. Van de Walle, *Phys. Rev. Lett.* **108**, 126404 (2012).
- [23] F. Karsai, P. Tiwald, R. Laskowski, F. Tran, D. Koller, S. Grafe, J. Burgdorfer, L. Wirtz, and P. Blaha, *Phys. Rev. B* **89**, 125429 (2014).
- [24] P. Tiwald, F. Karsai, R. Laskowski, S. Grafe, P. Blaha, J. Burgdorfer, and L. Wirtz, *Phys. Rev. B* **92**, 144107 (2015).
- [25] B. G. Janesko, *J. Chem. Phys.* **145**, 054703 (2016).
- [26] H. Pick, *Z. Phys.* **159**, 69 (1960).
- [27] A. Meyer and R. F. Wood, *Phys. Rev.* **133**, A1436 (1964).
- [28] A. Szabo and N. S. Ostlund, *Modern Quantum Chemistry: Introduction to Advanced Electronic Structure Theory* (Dover, Mineola, NY, 1989).
- [29] O. V. Gritsenko, P. R. T. Schipper, and E. J. Baerends, *J. Chem. Phys.* **107**, 5007 (1997).
- [30] A. D. Becke, *J. Chem. Phys.* **112**, 4020 (2000).
- [31] D. Cremer, *Mol. Phys.* **99**, 1899 (2001).
- [32] N. C. Handy and A. J. Cohen, *Mol. Phys.* **99**, 403 (2001).
- [33] J. W. Hollet and P. M. W. Gill, *J. Chem. Phys.* **134**, 114111 (2011).
- [34] E. R. Davidson and L. L. Jones, *J. Chem. Phys.* **37**, 1918 (1962).
- [35] E. J. Baerends, *Phys. Rev. Lett.* **87**, 133004 (2001).
- [36] J. S. Bell, *Physics* **1**, 195 (1964).
- [37] C. Kölmel and C. S. Ewig, *J. Phys. Chem. B* **105**, 8538 (2001).
- [38] L. H. Abu-Hassan and P. D. Townes, *J. Phys. C* **19**, 99 (1986).
- [39] O. V. Gritsenko, S. J. A. van Gisbergen, A. Görling, and E. J. Baerends, *J. Chem. Phys.* **113**, 8478 (2000).
- [40] K. Burke, *J. Chem. Phys.* **136**, 150901 (2012).
- [41] A. D. Becke, *J. Chem. Phys.* **140**, 18A301 (2014).
- [42] H. S. Yu, S. L. Li, and D. G. Truhlar, *J. Chem. Phys.* **145**, 130901 (2016).
- [43] C. D. Sherrill, M. S. Lee, and M. Head-Gordon, *Chem. Phys. Lett.* **302**, 425 (1999).
- [44] L. Noodleman, D. Post, and E. J. Baerends, *Chem. Phys.* **64**, 159 (1982).
- [45] K. Yamaguchi, F. Jensen, A. Dorigo, and K. N. Houk, *Chem. Phys. Lett.* **149**, 537 (1988).
- [46] A. Görling, *Phys. Rev. Lett.* **85**, 4229 (2000).

- [47] S. Grimme and M. Waletzke, *J. Chem. Phys.* **111**, 5645 (1999).
- [48] R. Rodríguez-Guzmán, K. W. Schmid, C. A. Jiménez-Hoyos, and G. E. Scuseria, *Phys. Rev. B* **85**, 245130 (2012).
- [49] T. Tsuchimochi and T. V. Voorhis, *J. Chem. Phys.* **142**, 124103 (2015).
- [50] J. P. Perdew, A. Ruzsinszky, L. A. Constantin, J. Sun, and G. I. Csonka, *J. Chem. Theor. Comput.* **5**, 902 (2009).
- [51] J. J. Phillips and J. E. Peralta, *J. Chem. Phys.* **135**, 184108 (2011).
- [52] E. Runge and E. K. U. Gross, *Phys. Rev. Lett.* **52**, 997 (1984).
- [53] R. Bauernschmitt and R. Ahlrichs, *J. Chem. Phys.* **104**, 9047 (1996).
- [54] M. E. Casida, C. Jamorski, K. C. Casida, and D. R. Salahub, *J. Chem. Phys.* **108**, 4439 (1998).
- [55] M. Caricato, G. W. Trucks, M. J. Frisch, and K. B. Wiberg, *J. Chem. Theor. Comput.* **6**, 370 (2010).
- [56] N. T. Maitra, *J. Chem. Phys.* **144**, 220901 (2016).
- [57] G. Onida, L. Reining, and A. Rubio, *Rev. Mod. Phys.* **74**, 601 (2002).
- [58] E. Rebolini, J. Toulouse, and A. Savin, in *Concepts and Methods in Modern Theoretical Chemistry: Electronic Structure and Reactivity*, edited by S. K. Ghosh and P. K. Chattaraj (CRC, Boca Raton, FL, 2013), pp. 367–389.
- [59] J. I. Fuks, A. Rubio, and N. T. Maitra, *Phys. Rev. A* **83**, 042501 (2011).
- [60] V. Bachler, *J. Comput. Chem.* **30**, 2087 (2009).
- [61] J. B. Foresman and H. B. Schlegel, in *Recent Experimental and Computational Advances in Molecular Spectroscopy*, edited by R. Fausto (Kluwer Academic, Dordrecht, 1993), pp. 11–26.
- [62] M. Rohrmüller, A. Hoffmann, C. Thierfelder, S. Herres-Pawlis, and W. G. Schmidt, *J. Comput. Chem.* **36**, 1672 (2015).
- [63] R. Kishi and M. Nakano, *J. Phys. Chem. A* **115**, 3565 (2011).
- [64] J. Fan, M. Seth, J. Autschbach, and T. Ziegler, *Inorg. Chem.* **47**, 11656 (2008).
- [65] Y. Shao, M. Head-Gordon, and A. I. Krylov, *J. Chem. Phys.* **118**, 4807 (2003).
- [66] R. Valero, F. Illas, and D. G. Truhlar, *J. Chem. Theor. Comput.* **7**, 3523 (2011).
- [67] C. A. Jiménez-Hoyos, T. M. Henderson, T. Tsuchimochi, and G. E. Scuseria, *J. Chem. Phys.* **136**, 164109 (2012).
- [68] J. E. Peralta, O. Hod, and G. E. Scuseria, *J. Chem. Theor. Comput.* **11**, 3661 (2015).
- [69] P. O. Dral and T. Clark, *J. Phys. Chem. A* **115**, 11303 (2011).
- [70] Gaussian Development Version, Revision I.02+, M. J. Frisch, G. W. Trucks, H. B. Schlegel, G. E. Scuseria, M. A. Robb, J. R. Cheeseman, G. Scalmani, V. Barone, B. Mennucci, G. A. Petersson, H. Nakatsuji, M. Caricato, X. Li, H. P. Hratchian, J. Bloino, B. G. Janesko, A. F. Izmaylov, A. Marenich, F. Lipparini, G. Zheng, J. L. Sonnenberg, W. Liang, M. Hada, M. Ehara, K. Toyota, R. Fukuda, J. Hasegawa, M. Ishida, T. Nakajima, Y. Honda, O. Kitao, H. Nakai, T. Vreven, K. Throssell, J. A. Montgomery, Jr., J. E. Peralta, F. Ogliaro, M. Bearpark, J. J. Heyd, E. Brothers, K. N. Kudin, V. N. Staroverov, T. Keith, R. Kobayashi, J. Normand, K. Raghavachari, A. Rendell, J. C. Burant, S. S. Iyengar, J. Tomasi, M. Cossi, N. Rega, J. M. Millam, M. Klene, J. E. Knox, J. B. Cross, V. Bakken, C. Adamo, J. Jaramillo, R. Gomperts, R. E. Stratmann, O. Yazyev, A. J. Austin, R. Cammi, C. Pomelli, J. W. Ochterski, R. L. Martin, K. Morokuma, V. G. Zakrzewski, G. A. Voth, P. Salvador, J. J. Dannenberg, S. Dapprich, P. V. Parandekar, N. J. Mayhall, A. D. Daniels, O. Farkas, J. B. Foresman, J. V. Ortiz, J. Cioslowski, and D. J. Fox, Gaussian, Inc., Wallingford CT, 2014.
- [71] A. Seidl, A. Görling, P. Vogl, J. A. Majewski, and M. Levy, *Phys. Rev. B* **53**, 3764 (1996).
- [72] A. V. Arbuznikov, M. Kaupp, and H. Bahmann, *J. Chem. Phys.* **124**, 204102 (2006).
- [73] H.-J. Ullrich, A. Uhlig, G. Geise, H. Horn, and H. Waltinger, *Mikrochim. Acta* **107**, 283 (1992).
- [74] W. J. Stevens, H. Basch, and M. Krauss, *J. Chem. Phys.* **81**, 6026 (1984).
- [75] S. H. Vosko, L. Wilk, and M. Nusair, *Can. J. Phys.* **58**, 1200 (1980).
- [76] J. C. Slater, *Adv. Quantum Chem.* **6**, 1 (1972).
- [77] J. P. Perdew, K. Burke, and M. Ernzerhof, *Phys. Rev. Lett.* **77**, 3865 (1996).
- [78] J. P. Perdew, in *Electronic Structure of Solids '91*, edited by P. Ziesche and H. Eschrig (Akademie Verlag, Berlin, 1991), pp. 11–20.
- [79] A. D. Becke, *J. Chem. Phys.* **107**, 8554 (1997).
- [80] P. J. Wilson, T. J. Bradley, and D. J. Tozer, *J. Chem. Phys.* **115**, 9233 (2001).
- [81] A. Vázquez-Mayagoitia, C. D. Sherrill, E. Aprà, and B. G. Sumpter, *J. Chem. Theor. Comput.* **6**, 727 (2010).
- [82] F. A. Hamprecht, A. J. Cohen, D. J. Tozer, and N. C. Handy, *J. Chem. Phys.* **109**, 6264 (1998).
- [83] A. D. Boese, N. L. Doltsinis, N. C. Handy, and M. Sprick, *J. Chem. Phys.* **112**, 1670 (2000).
- [84] A. D. Boese and N. C. Handy, *J. Chem. Phys.* **114**, 5497 (2001).
- [85] S. Grimme, *WIREs Comput. Molec. Sci.* **1**, 211 (2011).
- [86] J. Tao, J. P. Perdew, V. N. Staroverov, and G. E. Scuseria, *Phys. Rev. Lett.* **91**, 146401 (2003).
- [87] Y. Zhao and D. G. Truhlar, *J. Chem. Phys.* **125**, 194101 (2006).
- [88] J. P. Perdew, M. Ernzerhof, and K. Burke, *J. Chem. Phys.* **105**, 9982 (1996).
- [89] C. Adamo and V. Barone, *J. Chem. Phys.* **110**, 6158 (1999).
- [90] M. Ernzerhof and G. E. Scuseria, *J. Chem. Phys.* **110**, 5029 (1999).
- [91] A. J. Cohen and N. C. Handy, *Mol. Phys.* **99**, 607 (2001).
- [92] A. D. Becke, *Phys. Rev. A* **38**, 3098 (1988).
- [93] A. D. Becke, *J. Chem. Phys.* **98**, 1372 (1993).
- [94] A. D. Becke, *J. Chem. Phys.* **98**, 5648 (1993).
- [95] P. J. Stephens, F. J. Devlin, C. F. Chabalowski, and M. J. Frisch, *J. Phys. Chem.* **98**, 11623 (1994).
- [96] Y. Zhao and D. G. Truhlar, *J. Phys. Chem. A* **110**, 13126 (2006).
- [97] A. Austin, G. A. Petersson, M. J. Frisch, F. J. Dobek, G. Scalmani, and K. Throssell, *J. Chem. Theory Comput.* **8**, 4989 (2012).
- [98] J. Heyd, G. E. Scuseria, and M. Ernzerhof, *J. Chem. Phys.* **118**, 8207 (2003); **124**, 219906 (2006).
- [99] J. Heyd, J. E. Peralta, G. E. Scuseria, and R. L. Martin, *J. Chem. Phys.* **123**, 174101 (2005).
- [100] T. M. Henderson, A. F. Izmaylov, G. E. Scuseria, and A. Savin, *J. Chem. Theor. Comput.* **4**, 1254 (2008).
- [101] R. Baer, E. Livshits, and U. Salzner, *Annu. Rev. Phys. Chem.* **61**, 85 (2010).
- [102] O. A. Vydrov and G. E. Scuseria, *J. Chem. Phys.* **125**, 234109 (2006).



- [103] T. Benighaus, R. A. DiStasio Jr., R. C. Lochan, J.-D. Chai, and M. Head-Gordon, *J. Phys. Chem. A* **112**, 2702 (2008).
- [104] T. Yanai, D. P. Tew, and N. C. Handy, *Chem. Phys. Lett.* **393**, 51 (2004).
- [105] S. Hirata and M. Head-Gordon, *Chem. Phys. Lett.* **314**, 291 (1999).
- [106] A. F. Fix, F. U. Abuova, R. I. Eglitis, E. A. Kotomin, and A. T. Akilbekov, *Phys. Scr.* **86**, 035304 (2012).
- [107] A. Ruzsinszky, J. P. Perdew, G. I. Csonka, O. A. Vydrov, and G. E. Scuseria, *J. Chem. Phys.* **125**, 194112 (2006).
- [108] M. Marsman, J. Paier, A. Stroppa, and G. Kresse, *J. Phys.: Condens. Matter* **20**, 064201 (2008).
- [109] T. M. Henderson, A. F. Izmaylov, G. Scalmani, and G. E. Scuseria, *J. Chem. Phys.* **131**, 044108 (2009).
- [110] K. A. Nguyen, P. N. Day, and R. Pachter, *J. Chem. Phys.* **135**, 074109 (2011).